

AperTO - Archivio Istituzionale Open Access dell'Università di Torino

Hydroxyl radicals and oxidative stress: the dark side of Fe corrosion

This is the author's manuscript

Original Citation:

Availability:

This version is available <http://hdl.handle.net/2318/1732441> since 2023-03-01T13:45:00Z

Published version:

DOI:10.1016/j.colsurfb.2019.110542

Terms of use:

Open Access

Anyone can freely access the full text of works made available as "Open Access". Works made available under a Creative Commons license can be used according to the terms and conditions of said license. Use of all other works requires consent of the right holder (author or publisher) if not exempted from copyright protection by the applicable law.

(Article begins on next page)

Reactive Oxygen Species: the hidden face of biodegradable Fe-based alloys

E. Scarcello¹, M. Tomatis², F. Turci², A. Thomas³, P.J. Jacques³, D. Lison¹

¹ Louvain Centre for Toxicology and Applied Pharmacology (LTAP), Université catholique de Louvain, Avenue E. Mounier 53–bte B1.52.12, 1200 Brussels, Belgium.

² “G. Scansetti” Interdepartmental Center for Studies on Asbestos and Other Toxic Particulates, University of Torino, Via P. Giuria 9, 10125 Turin, Italy.

³ Institute of Mechanics, Materials and Civil Engineering (IMAP), Université catholique de Louvain, Place St Barbe 2, 1348 Louvain-la-Neuve, Belgium.

Abstract

The present work documents, for the first time, the ability of biodegradable Fe-based materials to produce hydroxyl radicals (OH•) during local corrosion and its cellular impact on endothelial cells.

The ability of Fe-based materials to generate OH• was documented by two complementary but independent acellular tests, i.e. terephthalate (TA) hydroxylation fluorescence and electron paramagnetic resonance (EPR) spectroscopy. The cellular responses were assessed *in vitro* on HUVECs and HAOECs using colorimetry and luminescence cytotoxicity assays. Cells were exposed directly to Fe powder, or to corrosion extracts. To confirm the cellular impact of OH•, mRNA expression of oxidative stress response genes (*HO-1* and *hGCLM*) was assessed in endothelial cells directly exposed to the same particles or corrosion extracts.

All tested Fe-based materials showed a strong potential to generate OH•, as a result of incomplete reduction of dissolved oxygen or via Fenton chemistry. The reduction of these signals in presence of D-mannitol confirmed their specificity for OH•. Only direct contact with Fe materials affected cell viability, indicating that released ions in corrosion extracts do not contribute to the cytotoxic activity. The expression of oxidative stress genes was dose-dependently increased 4 h after direct exposure to the particles, not to released ions. Pre-treatment with cytochalasin-D reduced cytotoxic and oxidative stress gene expression, indicating that endocytosis contributes to direct cell responses to Fe particles.

The demonstration of OH• production during corrosion and consequent oxidative stress in endothelial cells provides a new perspective on the biocompatibility of biodegradable Fe-based alloys. These findings will influence the future design of Fe-based implants, especially in vascular walls.

Keywords: oxidative stress, hydroxyl radicals, endothelial cells, coronary stent.

1. Introduction

During the last decade, biodegradable metallic alloys have been developed and investigated as alternatives for permanent implants, notably cardiovascular stents [1]. The most favorable and suitable coronary stent should, indeed, maintain its mechanical integrity only for the first 6–12 months, and be totally degraded after 12–24 months to avoid long-term restenosis or late thrombosis [2]. An ideal biodegradable material for coronary stent should, therefore, demonstrate a perfect compromise between degradation and mechanical performances. The first biodegradable biomaterials proposed were polymers from lactic acid, glycolic acid or caprolactone families but, while their biocompatibility and degradation rate appear adequate, their intrinsic mechanical properties are rather poor [3]. A more recent idea is to consider metals as biodegradable materials. Biodegradable magnesium-based alloys were first investigated for their better mechanical properties, but their specific strength remains weak compared to current permanent materials such as austenitic stainless steels (316L) [4]. The suitability of Fe as a biodegradable implant material has also been investigated. Fe combines a high strength, a high elastic modulus and a high ductility which can be helpful for the implantation of a stent when it needs to be plastically deformed. The first biodegradable Fe-based stent was made of Armco[®] iron (Fe > 99.8%) and implanted in the descending aorta of New Zealand white rabbits. No indication of local or systemic toxicity was detected, but the stents did not corrode completely over the 18 months follow-up period [5]. The addition of Mn to Fe may improve its performances, leading to excellent mechanical properties similar to 316L, combined with a degradation rate higher than pure Fe and tunable by varying the Mn content [3]. These degradation rates remain, however, one order of magnitude lower than those of Mg alloys. Other Fe-based alloys, including the austenitic Fe–Mn–C–Pd or TWIP (twinning-induced plasticity) steel alloys have been considered [6].

Immediately after implantation of a metallic stent in the artery, oxygen dissolved in the blood drives metal corrosion, generating free metal ions and associated degradation products. This process is complex as redox reactions generate not only ions, such as Fe²⁺ on the anodic side, but may also contribute to the formation of reactive oxygen species (ROS). While metal ions are released during corrosion, dissolved oxygen is concomitantly reduced in water (4 electrons) or, when the process is incomplete, in ROS such as OH• (3 electrons). OH• is the most damaging ROS which highly reacts with all biological macromolecules. It is one of the most potent oxidizing agents and has significant pro-inflammatory properties [7]. OH• can also be formed after Fe corrosion through a Fenton reaction in the presence of H₂O₂ present in the wounded arterial lumen [8].

Previous investigations on the biocompatibility of metallic materials often overlooked the complexity of these biodegradation phenomena and mostly focused on soluble ionic metallic forms released from the biocorrosion process [3, 6, 9, 10]. Most authors have so far concluded, based mostly on indirect cytotoxicity tests according to ISO standard 10993-5, that Fe-based alloys could be considered as nontoxic and biocompatible materials. Assuming that toxicity is exclusively driven by the solubilized metal ions represents, however, an over-simplification, and testing the response to ionic constituents or leachates

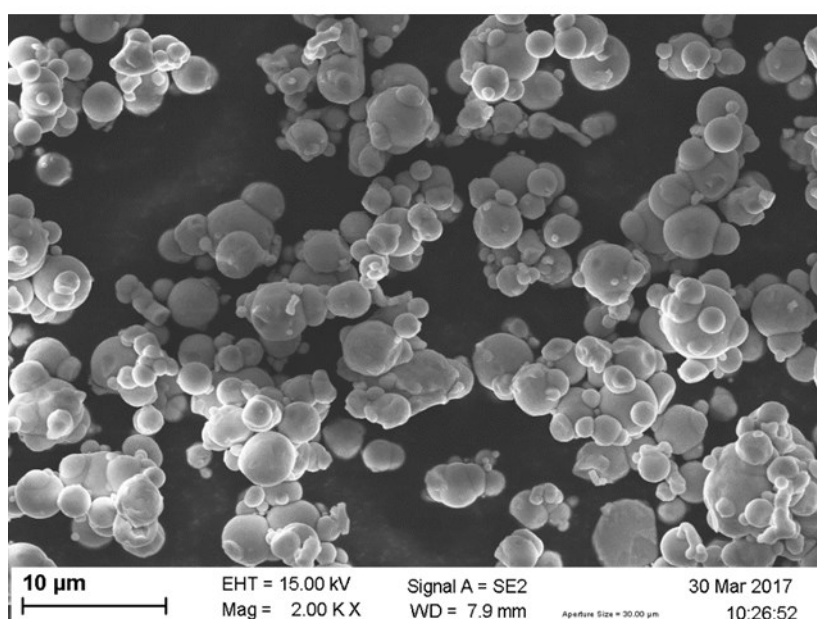
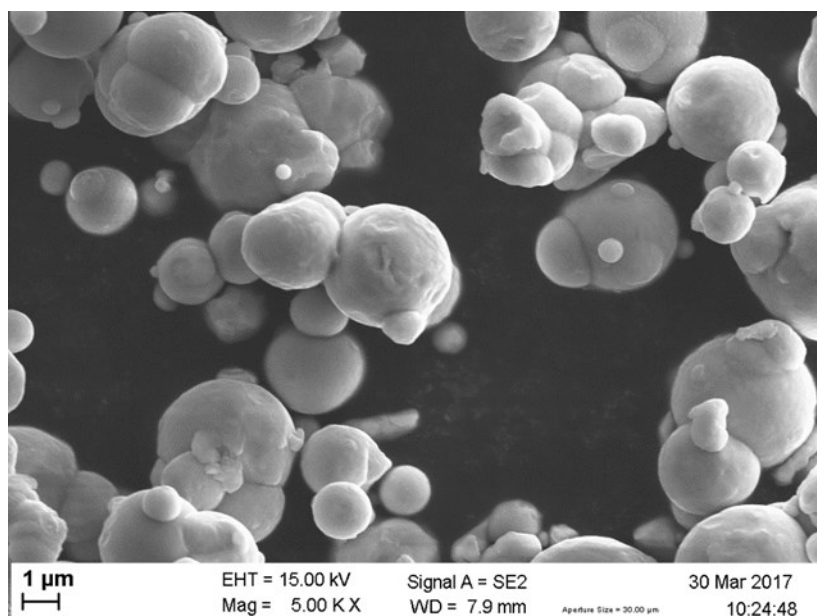
76 may not provide an appropriate approach. Specifically for Fe-based materials, the possible
77 role of ROS generated by dissolved oxygen deserves a specific attention in view of the
78 capacity of this element to contribute to catalytic redox cycling such as the well-known
79 Haber-Weiss reactions. For coronary stents, the possible implication of ROS appears very
80 relevant because of the critical role of oxidative stress in the atheromatous tissue. In
81 addition, balloon angioplasty and coronary stent implantation are associated with increased
82 vascular levels of ROS in conjunction with altered endothelial cell and smooth muscle cell
83 function [11]. Because corrosion is expected to occur during the whole life time of the
84 implant, ROS would be continuously formed at the implant surface, possibly resulting into
85 prolonged inflammation and unsuccessful healing of the surrounding tissues. Consequently,
86 understanding cellular reactions to implant-induced oxidative stress and inflammatory
87 activation is important to help prevent adverse responses to metallic stents [12].

88 While it is well established, in the field of inhalation toxicology, that metal particles can
89 release ROS, see e.g. [13], it is surprising that this aspect has not been well explored in the
90 field of biodegradable materials used for medical devices [14]. In this work we hypothesized
91 that OH• accompanying biocorrosion of Fe-based material are a source of toxicity for
92 endothelial cells. We specifically focused on the formation of OH• which appear the most
93 probable and deleterious ROS during the corrosion of Fe-based materials.

94 **2. Materials & Methods**

95 **2.1 Metallic materials**

96 Carbonyl iron powder (#44890, purity $\geq 99.5\%$) and iron chips (#267945, purity 99.98%)
97 were purchased from Sigma-Aldrich (St Louis, MO). Carbonyl iron particles were 5-9 μm
98 in spherical size (see SEM images, Supplementary data, Fig. S1). Other material sheets
99 were produced by melting iron (Alfa Aesar, 99.99%) or TWIP (FeMnC) in an arc furnace.
100 After a treatment of 10 minutes at 1000°C, the cast ingots were hot rolled to a thickness
101 lower than 2 mm. An Accutom[®] 5 automatic cut-off machine (Struer[®], Ballerup, Denmark)
102 was used to cut samples into 10x10 mm. Both sides of the samples were polished with SiC
103 water-proof paper 320 grits with water and then rinsed with 99.8 vol% absolute ethanol.
104 The specimens were finally ultrasonically washed in absolute ethanol for 10 min
105 immediately before ROS-generation tests. Micrometric crystalline silica particles were
106 Min-U-Sil[®] 5 (Berkeley Springs, West Virginia).



108

109 **Figure S1. Scanning Electron Microscope (SEM) images of carbonyl iron powder**
110 **(Sigma-Aldrich®).** The images were recorded using the SEM Ultra® 55 Zeiss at
111 different magnitude.

112 2.2 Electron paramagnetic resonance / spin trapping

113 The ability of the different samples to generate $\text{OH}\cdot$ was monitored by electron
114 paramagnetic resonance (EPR) spectroscopy with a Miniscope MS 100 (Magnettech,
115 Berlin, Germany) EPR spectrometer using DMPO as spin-trapping agent. The instrument
116 settings were as follows: modulation 1000 mG, scan range 120 G, center of field
117 approximately 3355 G.

118 **2.2.1 Carbon-centred free radicals detection during metal corrosion**

119 25 mg of the powder or a square massive sample (ARMCO® / Pure iron / TWIP) were
120 suspended in 1 ml of PBS (0.5 M, pH 7.4, Sigma-Aldrich, Milan, Italy) of sodium formate
121 (1.0 M, Sigma-Aldrich, Milan, Italy) and DMPO (0.04 M, Cayman Chemical Company,
122 Ann Arbor, Michigan). After 10, 30 and 60 min of incubation under continuous stirring,
123 aliquots of 50 µl were withdrawn, filtered (pore diameter 0.22 µm, Merck Chemicals SA,
124 Tullagreen, Carrigtwohill, Co. Cork, Ireland) and EPR spectra were recorded at room
125 temperature. Blanks were run in parallel in the absence of sample. Iron(II, III) oxide was
126 used a positive control [15]. All the measurements were performed in triplicate.

127 **2.2.2 Surface-driven Fenton reactivity (target molecule H₂O₂)**

128 25 mg of the powder or a square sample (ARMCO® / Pure iron / TWIP) were suspended in
129 1 ml of a phosphate-buffered saline (PBS 0.5 M, pH 7.4) containing DMPO (0.04 M) and
130 H₂O₂ (0.1 M). After 10, 30 and 60 min of incubation under continuous stirring, aliquots of
131 50 µl were withdrawn, filtered (0.22 µm) and EPR spectra were recorded at room
132 temperature. Blanks were run in parallel in the absence of sample. All the measurements
133 were performed in triplicate.

134 **2.3 Fluorimetric determination of hydroxyl radicals**

135 Disodium terephthalate (99%, Alfa Aesar, Tewksbury, MA) was dissolved in 0.01 M PBS
136 (pH 7.4) at a final concentration of 10 mM [16]. Iron powder or square samples were
137 suspended in TA solution (30 mg dust or a metal square piece / ml) and incubated for 30
138 min at 25°C under continuous stirring. In some assays, the OH• scavenger D-mannitol (75
139 mM, Sigma-Aldrich, St Louis, MO) was added to the reaction mixture. After incubation,
140 the suspensions were filtered on cellulose acetate membrane (0.22 µm) and the fluorescence
141 of the filtrate was measured on a SpectraMax i3x Multi-Mode microplate reader with an
142 excitation light $\lambda_{ex} = 324$ nm and reading the maximum emission intensity at $\lambda_{em} =$
143 425 nm.

144 **2.4 Controls in an oxygen-free environment**

145 The absence of OH• generation in an oxygen-free environment was verified for both
146 procedures described above (EPR and TA). In these assays, the aqueous buffered solution
147 containing DMPO or TA were deoxygenated by energetic bubbling of N₂ for 30 min before
148 adding samples and throughout the duration of the test.

149 **2.5 Cell culture**

150 Cell studies were performed with HUVEC and HAOEC endothelial cell lines (Cell
151 Application, Sigma-Aldrich, San Diego, CA) because endothelial cells are in direct contact
152 with the stent surface immediately after implantation [6]. HUVECs have been chosen
153 because they are arguably the most well-characterized primary human EC type [17] and
154 HAOECs as a stand-in for the arterial tunica intima [18]. The cells were cultured on 0.2%

155 gelatin-coated 75-cm² culture flasks (Corning Incorporated, Corning, NY) in Endothelial
156 Cell Growth Medium (Cell Application, Sigma-Aldrich, San Diego, CA) and maintained in
157 a humidified incubator (New Brunswick Galaxy[®] 170S) containing 5% CO₂ at 37°C. Cells
158 were grown to confluency and harvested by trypsinization. A maximum of 7 and 5 passages
159 was used for HUVECs and HAOECs, respectively, to maintain phenotypic characteristics
160 of endothelial cells. Cells were also routinely tested for the absence of Mycoplasma
161 infection (PCR Mycoplasma Test Kit I/RT, PromoKine, Huissen, the Netherlands).

162 **2.6 Direct cell viability assays**

163 The day of cell exposure, Fe particles were heated at 200°C (WTB, Binder[®] drying oven)
164 for 2 h for sterilization and destruction of any possible trace of endotoxin, and suspended in
165 cell culture medium at a stock concentration of 5 mg/ml. Immediately before cell exposure,
166 each particle suspension was diluted to final concentrations and vortexed. Direct cell
167 viability was assessed with the colorimetric WST-1 assay from Roche Diagnostics GmbH
168 (Mannheim, Germany) and the luminescent CellTiter-Glo[®] 2.0 assay from Promega Corp.
169 (Madison, WI). In the WST-1 assay, the amount of formazan dye formed is directly related
170 to the number of metabolically active cells. The assay was carried out as described in the
171 manufacturer's instruction. In brief, cells (2.10⁴ HUVECs or HAOECs) were seeded in 96-
172 well transparent plates and exposed the day after to different concentrations of iron powder
173 for 24 h. Cells were washed and incubated in fresh medium with 10% WST-1 reagent for
174 2h. Absorbance was measured at 450 nm, with 690 nm as reference, in a multiplate reader
175 (Infinite F200, Tecan[®]). Results are reported as relative WST-1 activity, where 1.0
176 corresponds to the absorbance measured in untreated control cultures. The CellTiter-Glo[®]
177 2.0 assay determines the number of viable cells in culture by quantitating the amount of
178 ATP which indicates the presence of metabolically active cells. In brief, cells (2.10⁴
179 HUVECs or HAOECs) were seeded in 96-well white plates and exposed as above. After
180 24h, the CellTiter-Glo reagent was added. Luminescence was read on a luminometer
181 (Victor[™] X4, PerkinElmer[®]). Results are reported as for WST-1.

182 For endocytosis inhibition studies, endothelial cells were treated with cytochalasin-D (2.5
183 μM, Sigma–Aldrich, St Louis, MO) 30 min before particle exposure. Min-U-Sil[®] 5 or Co
184 (II, III) oxide (Aldrich, St Luis, MO) were used as positive controls.

185 **2.7 Indirect cell viability assays**

186 HUVECs or HAOECs were also used to assess the *in vitro* cytotoxicity of corrosion extracts
187 generated after the immersion of increasing concentrations of iron powder in cell culture
188 medium for 24 h. The concentration of released Fe ions was quantified by inductively
189 coupled plasma - mass spectroscopy (ICP-MS) after filtration of the suspension (Amicon[®]
190 5000 NMWL, Millipore Corporation, Bedford). Endothelial cells were seeded in a 96-well
191 plate with a cell density of 2.10⁴ per well. After 24 h of incubation, the cell medium was
192 replaced by corrosion extracts and cells were further incubated for 24 h. The mitochondrial
193 activity or the ATP amount in viable cells were measured as described for the direct contact
194 test.

195 Indirect contact testing was also performed using a 96-well Transwell® chamber with 0.4
196 µm pore polycarbonate membrane insert (Corning® HTS, Sigma-Aldrich, St Luis, MO).
197 Cells were seeded in the lower chamber and allowed to adhere. After 24 h, increasing
198 concentrations of iron powder were added in the upper chamber. In this condition, only
199 degradation products released from the dust could reach cell culture at the bottom of the
200 well.

201 **2.8 Gene expression experiments**

202 Transcripts of oxidative stress response genes *HO-1* and *hGCLM* were measured in
203 HUVECs or HAOECs exposed to increasing concentrations of iron powder or corrosion
204 extracts for 4 h. Cells were washed twice and RNA was extracted with the TriPure Isolation
205 Reagent (Roche, Mannheim, Germany) according to the manufacturer's protocol, followed
206 by DNase treatment (Invitrogen Inc., Camarillo, CA). A quantity between 10 ng and 5 µg
207 of RNA was reverse transcribed by M-MLV-Reverse Transcriptase (Invitrogen) with 700
208 pmol/µl random hexamers (Eurogentec, Seraing, Belgium) in a final volume of 25 µl. The
209 resulting complementary DNA was then diluted 10-fold in sterile UltraPure® water
210 (Invitrogen) and used as template in subsequent real-time polymerase chain reactions
211 (PCR). Five microliters of diluted cDNA or standards were amplified using SYBR Green
212 technology in a total volume of 20 µl on a StepOnePlus™ Real-Time PCR System Thermal
213 Cycling Block (Applied Biosystems, Foster City, CA) according to the following program:
214 10 min 95°C and 40 cycles of (15 s 95°C + 1 min 60°C). After amplification, a melting
215 curve was generated and data analysis was performed with the StepOne™ Software v2.3
216 (Applied Biosystems). Primers for *HO-1*, *hGCLM* and *β-actin* were purchased from
217 Invitrogen Inc.

218 *β-actin*: (sense) 5' CCCGTGCTGCTGACCG G 3'
219 (antisense) 5' CGTCACCGGAGTCCATCAC 3';
220 *HO-1*: (sense) 5' GCAACAAAGTGCAAGATTCTGC 3'
221 (antisense) 5' GCTGTAGGGCTTTATGCCATGT 3';
222 *hGCLM*: (sense) 5' CAGCCTTACTGGGAGGAATTAGAA 3'
223 (antisense) 5' TTA CTATTTGGTTTTACCTGTGCC 3'.

224 Results were calculated as a ratio of *HO-1* or *hGCLM* expression to the expression of the
225 reference gene, *β-actin*.

226 **2.9 Antioxidants**

227 Endothelial cells were treated with D-mannitol (125 mM), D-sorbitol (1.5 mM), sodium
228 formate (10 mM), N-acetyl-L-cysteine (NAC, 5 µM), uric acid (1 mM), ascorbic acid (250
229 µg/ml), 2,6-di-tert-butyl-4-methylphenol (BHT, 0.01 mM), trolox (5 µM) or catalase (250
230 units/ml) immediately prior to iron powder exposure as described in section [2.6](#). All
231 antioxidants were purchased from Sigma-Aldrich (St Louis, MO).

232 **2.10 Statistical analysis**

233 Data are presented as means \pm standard error of the mean (S.E.M.) of independent
234 experiments (N) conducted in replicates (n). The data were analyzed with GraphPad Prism
235 (GraphPad software, La Jolla, CA) and OriginPro9.0 software (OriginLab Corp.,
236 Northampton, MA). Differences between groups were analyzed by one-way analysis of
237 variance (ANOVA) followed by a post-hoc Dunnett's pairwise comparison test. Differences
238 with p value < 0.05 compared to control group were considered statistically significant.

239

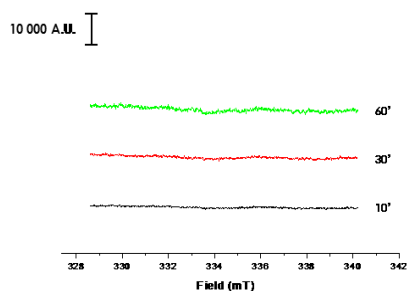
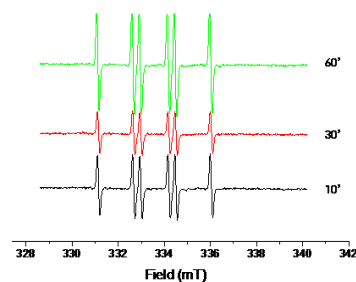
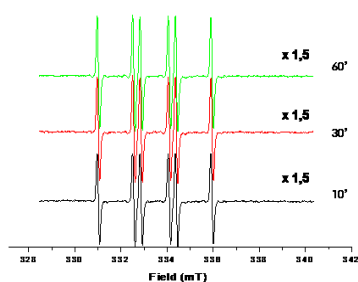
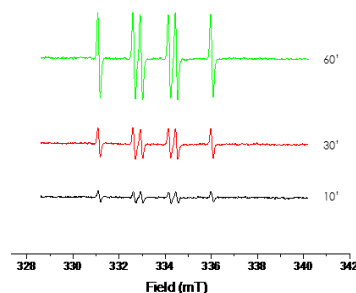
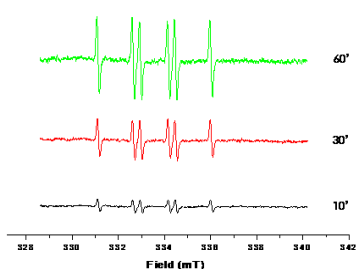
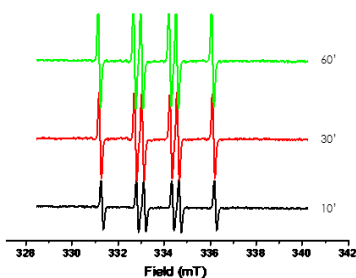
240

3. Results

241

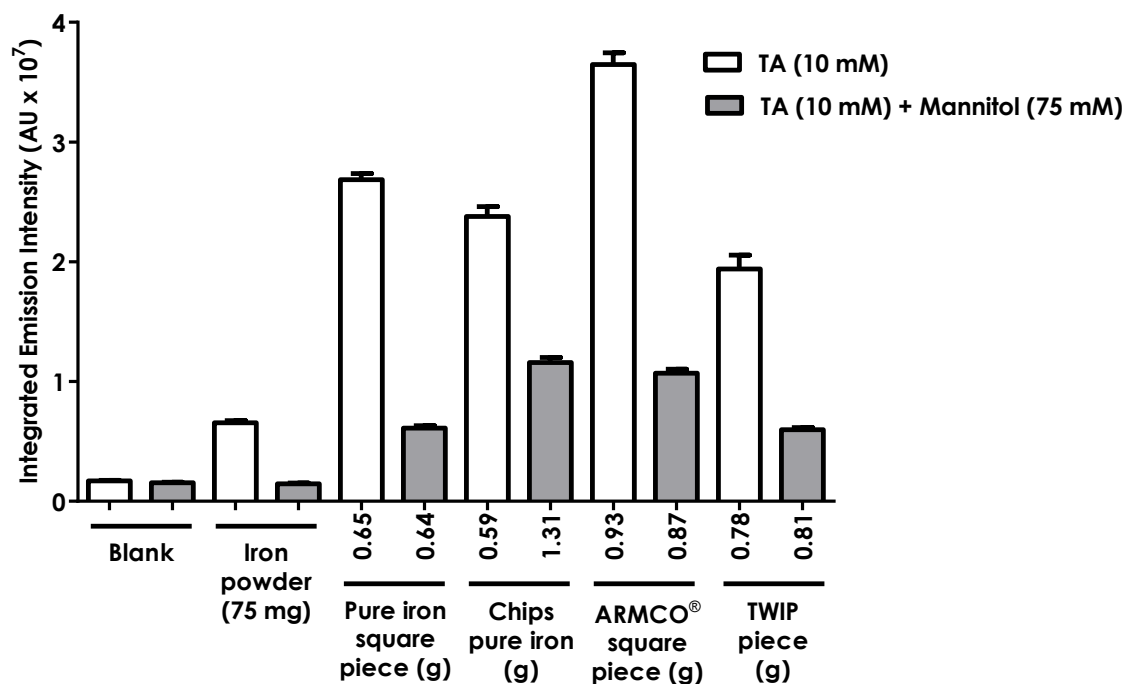
3.1 Fe-based materials generate hydroxyl radicals

242 Our first goal was to determine the ability of Fe-based materials to release $\text{OH}\cdot$ in aqueous
243 conditions. The formation of $\text{OH}\cdot$ during the corrosion of Fe-based materials was assessed
244 by monitoring the formation of carbon-centered free radicals in the presence of formate
245 [19]. The cleavage of a C–H bond was detected by spin trapping and quantified by EPR
246 spectroscopy. Representative EPR spectra of the $[\text{DMPO}-\text{CO}_2]\cdot-$ adducts indicated that iron
247 powder (Fig. 1b), pure iron piece (Fig. 1c), pure iron chips (Fig. 1d), ARMCO[®] piece (Fig.
248 1e) and TWIP piece (Fig. 1f) strongly generated carboxyl radicals ($\cdot\text{CO}_2^-$) in solution. No
249 signal was detected in the absence of Fe material (blank) (Fig. 1a). The strong reactivity of
250 Fe-based materials was maintained over time, up to 60 min.

a. Blank**b. Iron powder****c. Pure iron piece****d. Pure iron chips****e. ARMCO piece****f. TWIP piece**

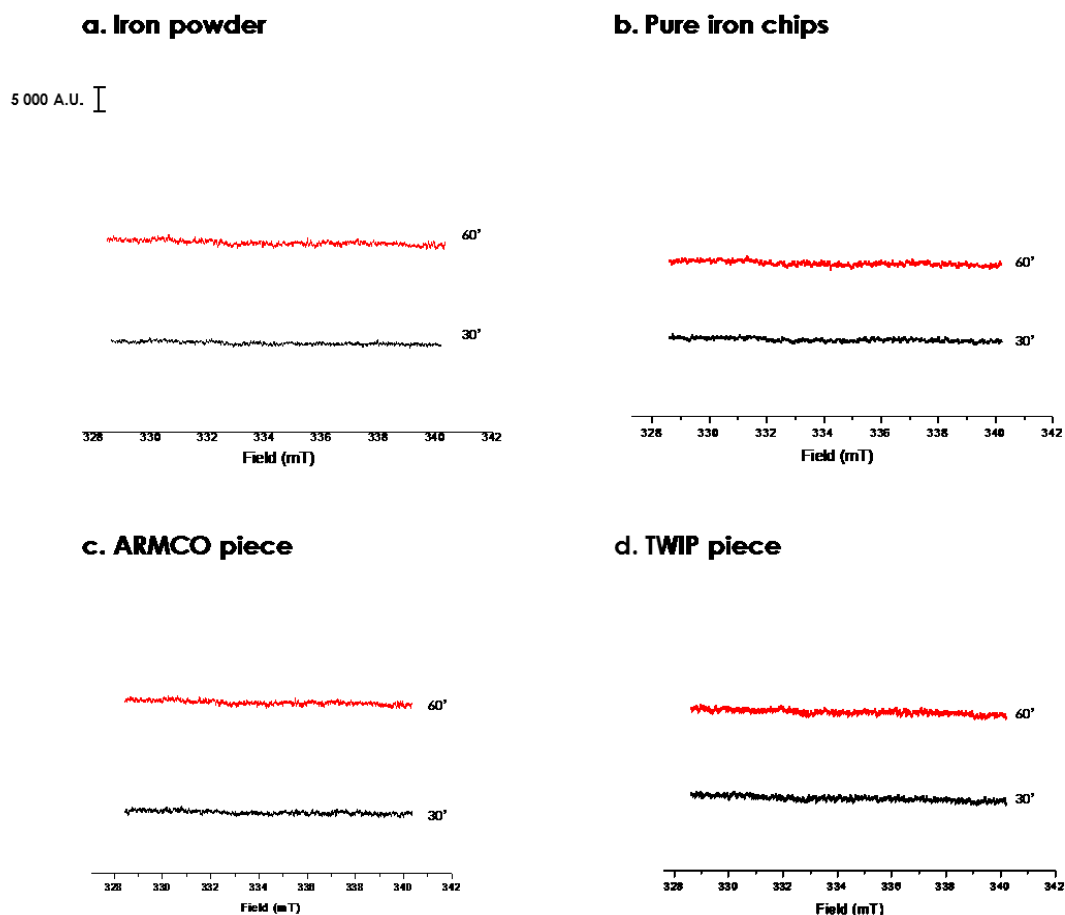
251 **Figure 1. Surface driven release of hydroxyl radicals from the corrosion of Fe-based**
 252 **materials.** EPR spectra recorded on suspensions of iron powder (75 mg, **b**), pure iron
 253 piece (10x10x1.5 mm, **c**), pure iron chips (670.6 mg, **d**), ARMCO® piece (10x10x1.5
 254 mm, **e**) and TWIP piece (10x10x1.5 mm, **f**) compared to blank (**a**) in a sodium formate-
 255 buffered solution in the presence of DMPO as spin-trapping agent. Aliquots of 50 µl of
 256 suspension were withdrawn after 10, 30 and 60 min of incubation under continuous
 257 stirring at room temperature, filtered and analysed for EPR spectra.
 258 The panel shows a representative spectrum out of at least three experiments.
 259 x 1,5 means one and a half EPR signal intensity.
 260

261 In order to support the EPR results, we applied a complementary test using a different
 262 readout, i.e. the capacity of OH• to hydroxylate TA. Compared to the blank (Fig. 2), all Fe-
 263 based samples were able to hydroxylate TA, regardless of weight, form or Fe content. The
 264 specificity of the TA measurement was verified by adding D-mannitol, an OH• scavenger
 265 frequently used in biological systems [20]. D-mannitol significantly reduced the signal,
 266 confirming the generation of OH• during Fe-based materials corrosion.



267 **Figure 2. Corrosion of Fe-based materials generates hydroxyl radicals.** Fluorimetric
 268 determination of hydroxyl radicals released from Fe-based materials using the
 269 terephthalate (TA) assay. Samples were immersed in a buffered (PBS) solution of
 270 disodium terephthalate (10 mM) for 30 min at RT under continuous stirring in the
 271 absence/presence of D-mannitol, an hydroxyl radical scavenger (75 mM).
 272 Supernatant was recovered, filtered and the fluorescence was measured (excitation
 273 $\lambda_{ex} = 324 \text{ nm}$, emission $\lambda_{em} = 425 \text{ nm}$). Data are means \pm SEM (N=4, n=3).
 274

275 To confirm that dissolved oxygen drives the generation of OH•, spin trapping and
 276 fluorimetric measurements were performed in an oxygen-free environment. The absence of
 277 oxygen completely suppressed the corrosion mechanism and the generation of OH•
 278 (Supplementary data, Fig. S2).



280
281
282
283
284
285
286
287
288
289

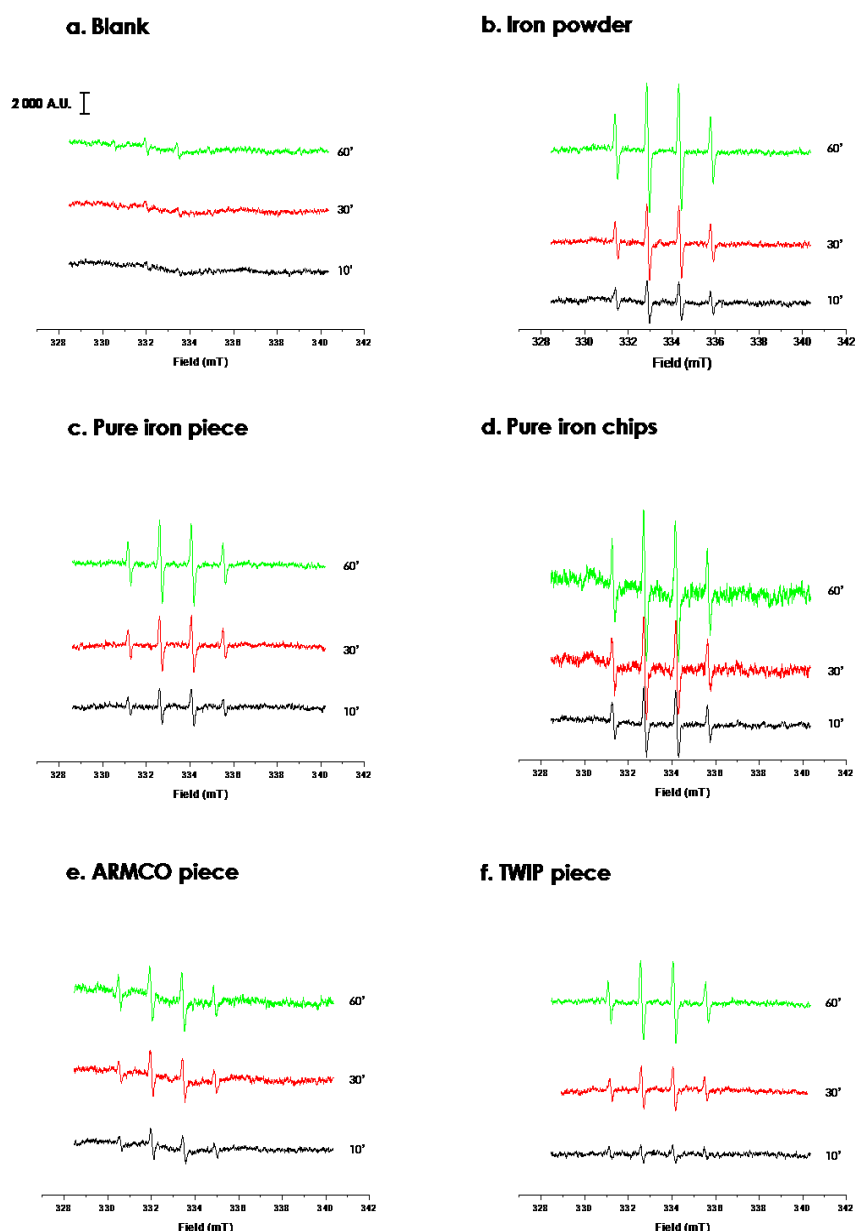
Figure S2. Generation of hydroxyl radicals by Fe-based materials is oxygen-dependent. EPR spectra recorded on suspensions of iron powder (75 mg, **a**), pure iron chips (632 mg, **b**), ARMCO[®] piece (10x10x1.5 mm, **c**) and TWIP piece (10x10x1.5 mm, **d**) in a aqueous buffered solution in the presence of DMPO as spin-trapping agent. The solution was previously deoxygenated by vigorously bubbling N₂ for 30 min; the oxygen-free environment was maintained for the duration of the test. Aliquots of 50 µl of suspension were withdrawn after 10, 30 and 60 min of incubation under continuous stirring at room temperature, filtered and analysed for EPR spectra.

290

291 When Fe cations are generated in the presence of hydrogen peroxide, additional reactions
292 known as the Fenton reaction (Eq.¹) can take place, also leading to the generation of OH• :



294 Representative EPR spectra of [DMPO–HO]–adduct recorded in the presence of H₂O₂ are
295 reported (Fig. **3b-d**). No signal was detected in the absence of Fe material (Fig. **3a**). A time-
296 dependent increase in the intensity of the EPR signal was observed with all tested samples.



298
299
300
301
302
303
304
305
306

Figure 3. Fenton-mediated generation of hydroxyl radicals during corrosion of Fe-based materials. EPR spectra recorded on suspensions of iron powder (75 mg, **b**), pure iron piece (10x10x1.5 mm, **c**), pure iron chips (2.19 g, **d**), ARMCO[®] piece (10x10x1.5 mm, **e**) and TWIP piece (10x10x1.5 mm, **f**) compared to blank (**a**) in a aqueous buffered solution in the presence of H₂O₂ (0,1M) and DMPO as spin-trapping agent. Aliquots of 50 μ l of suspension were withdrawn after 10, 30 and 60 min of incubation under continuous stirring at room temperature, filtered and analysed for EPR spectra.

The panel shows a representative spectrum out of at least three experiments.

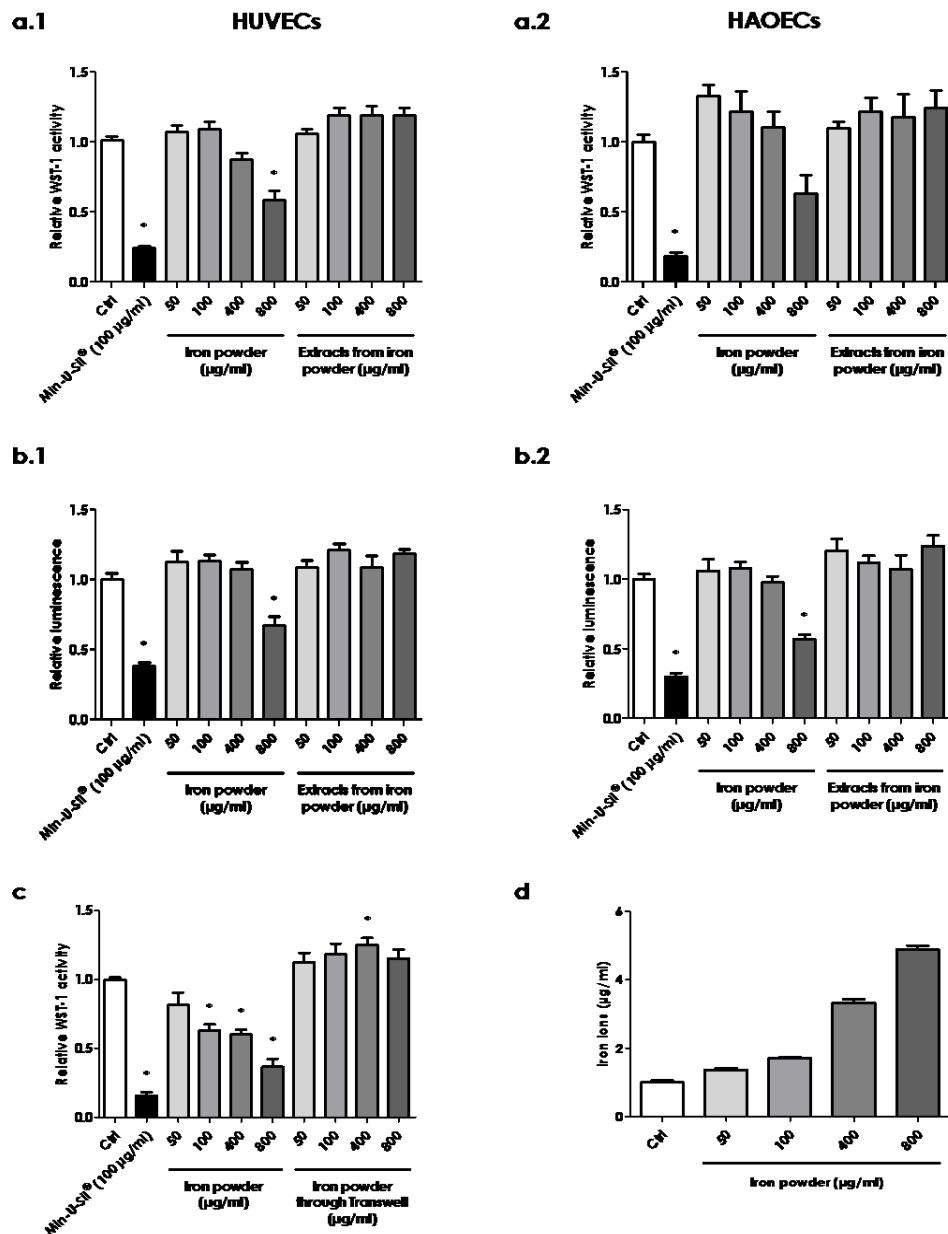
307

308 Alternative reactions could also lead to radical adduct artifacts such as nucleophilic addition
309 of water at the nitrene carbon (or C-2 position) of DMPO in the presence of Fe(III) ions
310 [21]. Hence, we recorded the [DMPO–HO]–adduct without H₂O₂ and no signal was

311 detected, demonstrating that, under our experimental conditions, DMPO exclusively forms
312 the radical adduct by trapping the OH• (data not shown). We, therefore, concluded that the
313 corrosion of Fe-based materials generates OH•.

314 **3.2 Direct cellular contact with Fe powder induces endothelial responses**

315 We next used Fe powder to assess the responses of endothelial cells. We reasoned that if
316 OH• are generated, they need, due to their short half-life, an intimate contact with cells to
317 exert a cytotoxic activity. We, therefore, compared the response to Fe powder in direct and
318 indirect cytotoxicity assays, hypothesizing that only the direct assay could capture the
319 activity of OH•. Experiments were carried out in two cell lines, HUVECs and HAOECs,
320 using two cytotoxicity tests based on different principles, i.e. colorimetry and luminescence.
321 Both assays showed that only direct contact with Fe powder significantly and dose-
322 dependently affected the viability of endothelial cells after 24 h exposure. In contrast,
323 indirect assays (corrosion extracts or Transwell exposure) did not reveal a cytotoxic activity
324 of the Fe powder (Fig. **4a, b, c**).



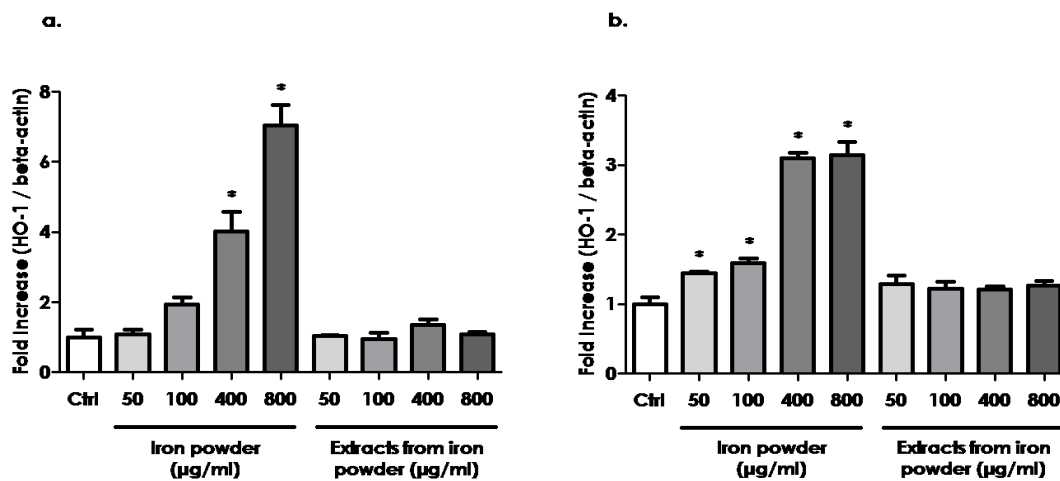
325 **Figure 4. Direct exposure to iron powder affects endothelial cell viability.** Cells (2.10^4)
 326 HUVECs or HAOECs) were seeded in 96-well transparent or white plates and exposed
 327 the day after to different concentrations of iron powder or corrosion extracts for 24 h.
 328 Extracts were obtained from culture medium incubated during 24 h with increasing
 329 concentrations of iron powder. Supernatants were collected and centrifuged. The
 330 chemical concentration of released iron ions was quantified by inductively coupled
 331 plasma - mass spectroscopy (ICP-MS) after filtration of the suspension (d). In some
 332 experiments a 96-well Transwell[®] chamber with 0.4 μm pore polycarbonate
 333 membrane insert was used, where cells were seeded in the lower chamber allowing
 334 to adhere for 24 h and increasing concentrations of iron powder were added in the
 335 upper chamber (c). The cells were washed and incubated in fresh medium with 10%
 336 WST-1 reagent for 2 h. Absorbance was measured at 450 nm, with 690 nm as
 337 reference, in a multiplate reader (a.1, b.1, c). The white plate was replenished
 338 with fresh medium with the CellTiter-Glo[®] reagent and luminescence was read on a
 339 luminometer (a.2, b.2). Results are reported as relative WST-1 activity or luminescence

340 (R.L.U.), where 1.0 corresponds to the value measured in untreated control cultures.
341 Min-U-Sil[®] 5 was used as positive control. Data are means \pm SEM for at least three
342 samples (N=4), * $p < 0.05$.

343

344 To further support the response of endothelial cells to OH \bullet when in contact with Fe powder,
345 we documented the oxidative stress response by monitoring the expression of heme
346 oxygenase-1 (*HO-1*). *HO-1* was increased dose-dependently 4 h after direct exposure,
347 whereas corrosion extract exposure did not induce such a response (Fig. 5). Similar results
348 were obtained for another oxidative stress marker, human glutamate cysteine ligase
349 modifier subunit (*hGCLM*, Supplementary data, Fig. S3). These results supported the
350 concept that OH \bullet induce oxidative stress responses in endothelial cells.

351



352

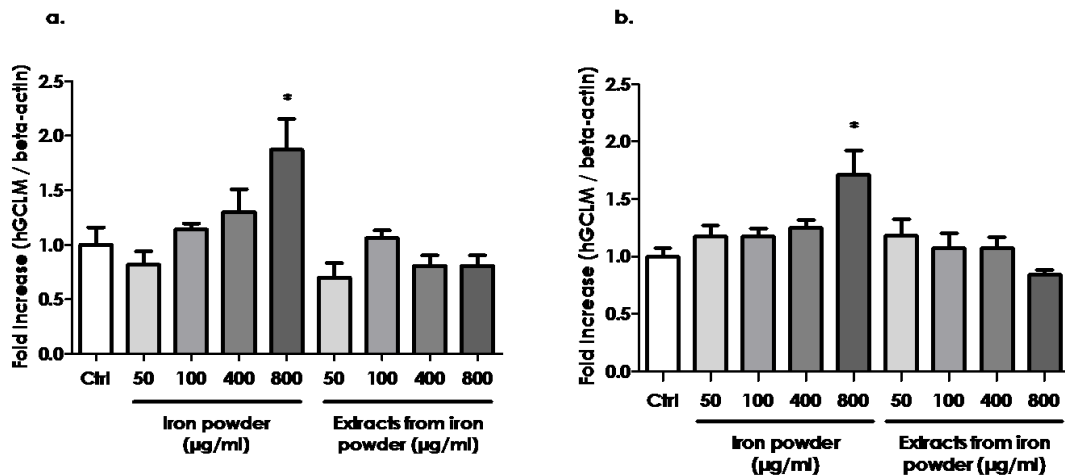
353 **Figure 5. Corrosion of iron powder induces oxidative stress in EC.** HUVECs (a) or
354 HAOECs (b) were exposed to different concentrations of iron powder or corrosion
355 extracts for 4 h. RNA was extracted and reverse transcribed for real-time polymerase
356 chain reactions (PCR). Values of heme oxygenase-1 (HO-1) mRNA were normalized
357 to β -actin amplified from the same samples and are presented as fold increase
358 compared to untreated cells. Data are means \pm SEM, * $p < 0.05$ (N=2, n=4).
359

360

361 We tried to protect endothelial cells from oxidative stress with antioxidants as described in
362 section 2.9. No evidence of HUVECs or HAOECs protection from OH \bullet was recorded, as
363 assessed by cytotoxicity or oxidative stress genes induction.

364 To clarify the mechanism of their response to Fe particles, endothelial cells were pre-treated
365 with cytochalasin-D, an inhibitor of actin polymerization that blocks >90% of endocytosis
366 [22]. When cells were pre-treated with cytochalasin-D no cytotoxic or oxidative stress
367 gene expression was observed (Fig. 6a, b).

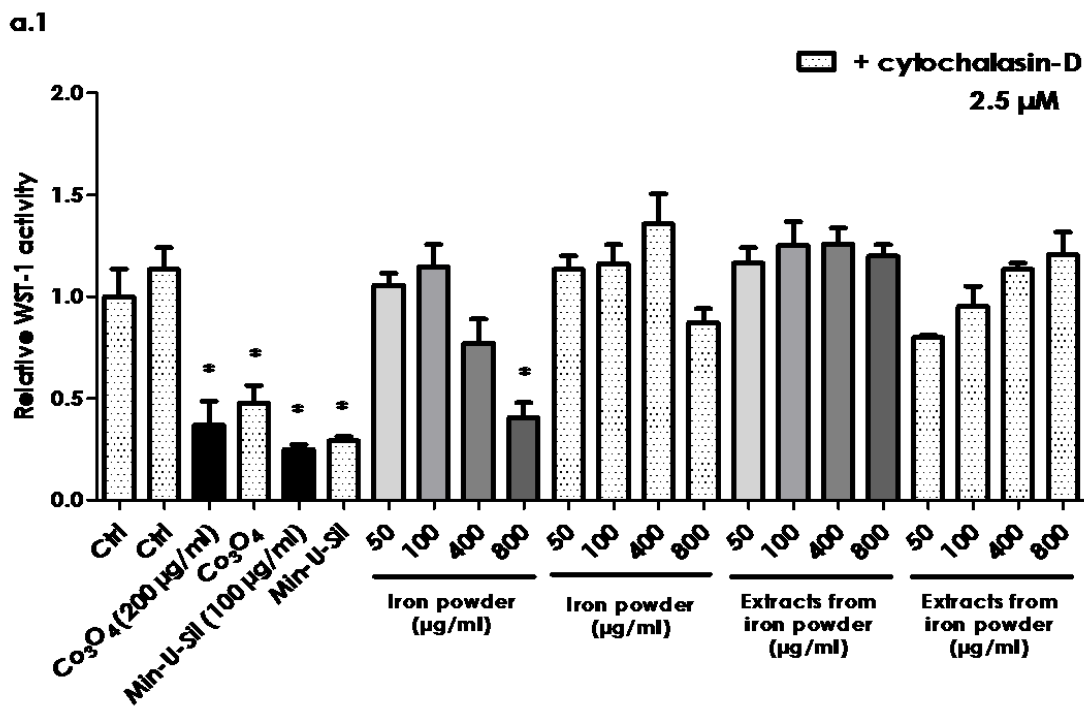
368

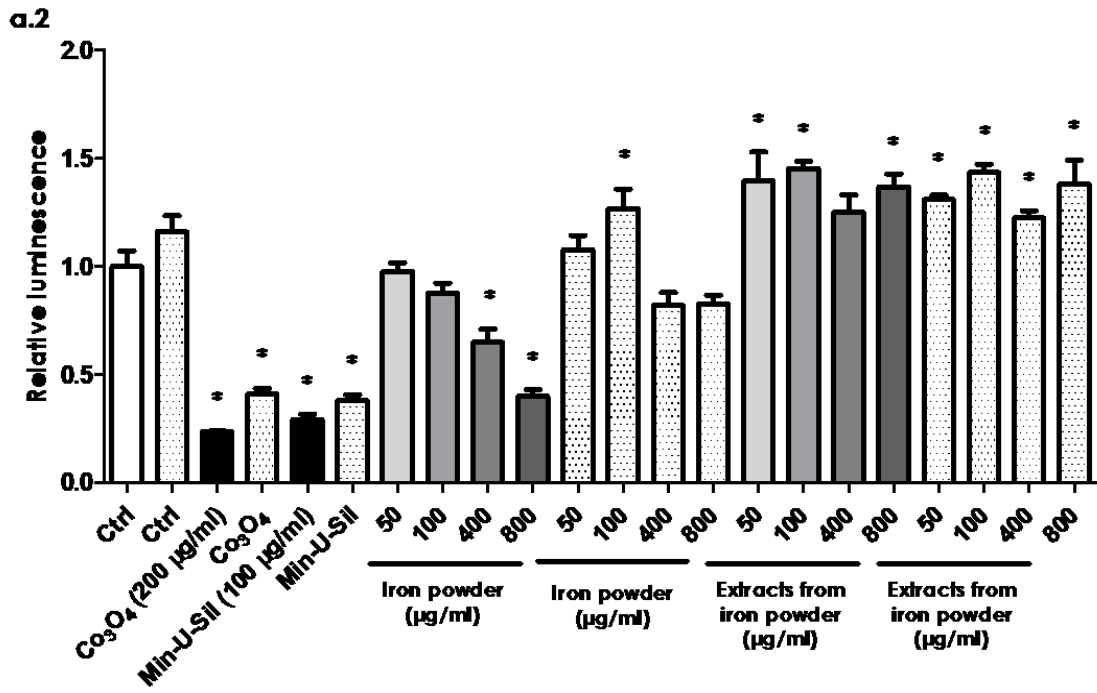


370

371
372
373
374
375
376
377

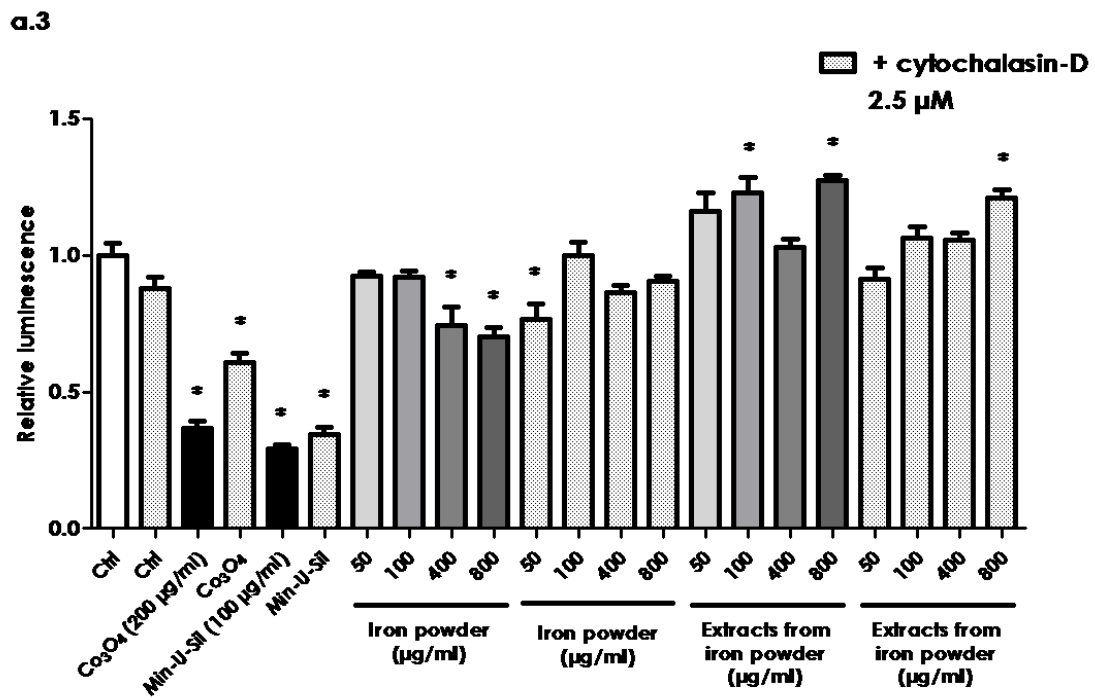
Figure S3. Corrosion of iron powder induces oxidative stress in EC. HUVECs (a) or HAOECs (b) were exposed to different concentrations of iron powder or corrosion extracts for 4 h. RNA was extracted and reverse transcribed for real-time polymerase chain reactions (PCR). Values of glutamate cysteine ligase modifier subunit (hGCLM) mRNA were normalized to β -actin amplified from the same samples and are presented as fold increase compared to untreated cells. Data are means \pm SEM, * $p < 0.05$ (N=1, n=4).

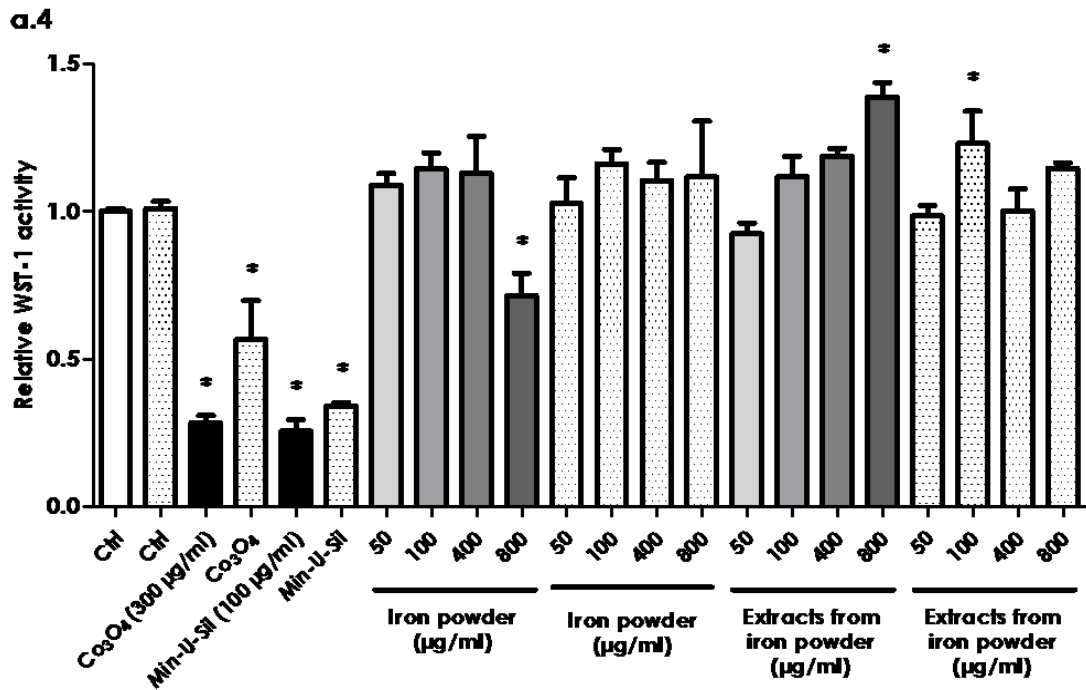




378

379





380

381 **Figure 6. Only iron powder endocytosis induced endothelial cytotoxicity.** Cells (2.10^4
 382 HUVECs or HAOECs) were seeded in 96-well transparent or white plates and exposed
 383 the day after to different concentrations of iron powder or corrosion extracts with or
 384 without pre-exposure with cytochalasin-D ($2.5 \mu\text{M}$, 30 min before particle exposure).
 385 After 24 h, the cells were washed and incubated in fresh medium with 10% WST-1
 386 reagent for 2 h. Absorbance was measured at 450 nm, with 690 nm as reference, in
 387 a multiplate reader (a.1, 3). The white plate was replenished with fresh medium with
 388 the CellTiter-Glo[®] reagent and luminescence was read on a luminometer (a.2, 4).
 389 Results are reported as relative WST-1 activity or luminescence (R.L.U.), where 1.0
 390 corresponds to the value measured in untreated control cultures. Min-U-Sil[®] 5 and
 391 Co(II, III) oxide were used as positive controls. Data are means \pm SEM for at least three
 392 samples (N=4), * $p < 0.05$.
 393

394

395 4. Discussion

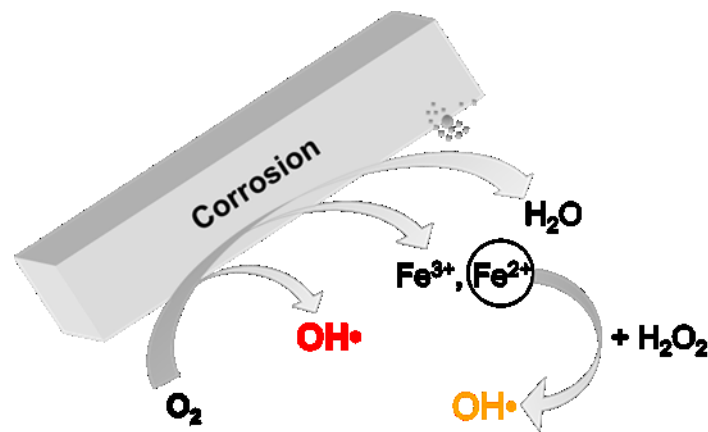
396 We documented, for the first time, the ability of biodegradable Fe-based materials to
 397 produce $\text{OH}\cdot$ during corrosion. Metallic materials that undergo corrosion, release
 398 degradation products at the implanted site thus constantly causing the formation of ROS
 399 [14], but no previous study had been carried out in order to evaluate the $\text{OH}\cdot$ -producing
 400 activity of biodegradable Fe-based alloys. This finding is important because it sheds a new
 401 light on the biocompatibility of Fe-based alloys investigated as implant. These have been
 402 generally considered as having good biocompatibility properties mostly based on indirect
 403 contact cellular tests [3, 6, 9, 23, 24]. These assays can, however, not capture the cytotoxic
 404 activity of the short-lived oxygen species.

405 To cover a wide range of implanted materials used in medicine and their different surface
406 reactivity, we tested several samples of Fe-based materials differing in shape, size, surface
407 area, roughness and composition. All samples examined here showed a strong potential to
408 generate OH• in acellular systems, via EPR and TA hydroxylation assays, two
409 complementary techniques [25]. Any quantitative comparison of OH• yields must, however,
410 be considered carefully because the samples were not tested under similar conditions of
411 dose, surface area, geometry and Fe content.

412 Implant corrosion releases degradation products that can be found in various forms,
413 including free metallic ions, colloidal complexes, inorganic metal salts or oxides and wear
414 particles [14]. Particle size and shape change with the passage of time and corrosion
415 particles can further contribute to corrosion, as the surface in contact with the surrounding
416 fluids becomes larger [26]. Incomplete reduction of dissolved oxygen could produce ROS,
417 such as OH•, on material surface that will immediately react with almost every molecule in
418 its environment. It can also be expected that local corrosion of Fe implants releases metal
419 ions which undergo the Fenton reaction in presence of H₂O₂, also present in the wounded
420 area. As biocorrosion persists through the life of the implant, OH• are likely to be
421 continuously formed at the implant site, worsening the local oxidative stress levels of the
422 diseased tissue. This could influence the success of the device implantation and the healing
423 of the surrounding tissues [27]. Small debris as result of metal degradation migrate in the
424 tissue surrounding the material and are immediately phagocytosed, whereas metal
425 nanoparticles can pass through the cell plasma membrane mainly by diffusion or
426 endocytosis [28]. Hence, ROS derived from the material may cause intracellular oxidative
427 damage, including to the nucleus proteins and lipids, resulting in inhibition of DNA repair
428 pathways, impair of nuclear signal transduction and defective gene expression [29]. We
429 found that endocytosed Fe particles directly affected endothelial cells viability probably via
430 intra-cellular corrosion and OH• production. This toxicity mechanism could explain that
431 antioxidants, able to scavenge OH• in a cell free environment were unable to protect
432 endothelial cells. Indeed, OH• would be mostly produced in a microenvironment poorly
433 accessible to water-soluble antioxidants, possibly after endocytosis. Moreover, during the
434 24 h cell exposure, antioxidant molecules may have reacted with cell culture medium
435 components and lead to different forms of antioxidant, or simply degrade, whereas iron
436 particles are immediately cell-internalized. It is possible that using a massive sample (e.g.
437 cube or disk [30]) instead of our model particles, may lead to different results, because the
438 degradation rate of the bulk material during a cell culture test is expected to cause less
439 particle formation and consequent endocytosis.

440 Overall, acellular results showed that dissolved oxygen drives the corrosion of Fe-based
441 materials and generates OH• by two different ways, directly on the metal surface or through
442 Fe ions released that undergo a Fenton reaction, as shown in Fig. 7. Direct OH• release
443 emerges as the most significant to induce cell toxicity or oxidative stress as exposure to
444 extracts, that include iron ions able to react with the H₂O₂, did not affect cell responses.

445



446

447 **Figure 7 Summary of mechanism of OH• from the corrosion of Fe-based materials.**

448 OH• are directly generated from the incomplete reduction of dissolved oxygen
449 (surface driven release, in red) or mediated by Fe ions that react with H₂O₂ (Fenton-
450 mediated generation, in yellow).

451

452 The mechanisms highlighted here can act as a first approximation of the biodegradation of
453 a Fe-based implant and its impact on surrounding tissues. These results represent a
454 particularly interesting aspect because, until now, little was known about biomaterials and
455 oxidative stress, and the mechanism underlying metal toxicity is still not fully understood
456 [14]. The present data suggest that some of the classic experiments used for evaluating *in*
457 *vitro* biomaterials toxicity, such as indirect contact test [3, 6, 9, 23, 24, 31], are not
458 appropriate to capture the impact of implanted biodegradable Fe-based materials on
459 surrounding tissue. In the light of our results, assuming that toxicity is exclusively driven
460 by the solubilized metal ions represents an over-simplification, missing the contribution of
461 the short-lived ROS. In addition, our data indicate that oxidative stress might contribute to
462 the toxicity of biodegradable Fe-based materials and this aspect appears particularly
463 relevant to take into account for an atheromatous tissue already submitted to oxidative stress
464 [32].

465 5. Acknowledgments

466 This work was supported by an ARC grant (principal promoter Pascal J. JACQUES).

467

468 **References**

- 469 1. Mantovani, M.M.a.D., *Biodegradable Metals for Cardiovascular Stent Application: Interests and New Opportunities*. International Journal of Molecular Sciences, 2011. 470 **12**: p. 4250-4270.
- 471
- 472 2. Francis, A., et al., *Iron and iron-based alloys for temporary cardiovascular* 473 *applications*. J Mater Sci Mater Med, 2015. **26**(3): p. 138.
- 474 3. Hendra Hermawan, A.P., Dominique Dube, Jacques Couet, Diego Mantovani, *Fe–Mn* 475 *alloys for metallic biodegradable stents: Degradation and cell viability studies*. Acta 476 Biomaterialia, 2010. **6**: p. 1852-1860.
- 477 4. B Heublein, R.R., V Kaese, M Niemeyer, W Hartung, A Haverich, *Biocorrosion of* 478 *magnesium alloys: a new principle in cardiovascular implant technology?* Heart 479 Journal, 2003. **89**: p. 651-656.
- 480 5. M Peuster, P.W., M Brüggemann, M Ehlerding, K Seidler, C Fink, H Brauer, A Fischer, 481 G Hausdorf, *A novel approach to temporary stenting: degradable cardiovascular* 482 *stents produced from corrodible metal—results 6–18 months after implantation into* 483 *New Zealand white rabbits*. Heart Journal, 2001. **86**: p. 563-569.
- 484 6. Michael Schinhammer, I.G., Anja C. Hänzi, Peter J. Uggowitz, *On the* 485 *cytocompatibility of biodegradable Fe-based alloys*. Materials Science and 486 Engineering C, 2013. **33**: p. 782-789.
- 487 7. H. Ahsan, A.A.a.R.A., *Oxygen free radicals and systemic autoimmunity*. Clinical and 488 Experimental Immunology, 2003. **131**: p. 398-404.
- 489 8. van der Vliet, A. and Y.M. Janssen-Heininger, *Hydrogen peroxide as a damage signal* 490 *in tissue injury and inflammation: murderer, mediator, or messenger?* J Cell Biochem, 491 2014. **115**(3): p. 427-35.
- 492 9. Huang, T., et al., *Fe-Au and Fe-Ag composites as candidates for biodegradable stent* 493 *materials*. J Biomed Mater Res B Appl Biomater, 2016. **104**(2): p. 225-40.
- 494 10. Zhou, W.R., et al., *Mechanical property, biocorrosion and in vitro biocompatibility* 495 *evaluations of Mg-Li-(Al)-(RE) alloys for future cardiovascular stent application*. 496 Acta Biomater, 2013. **9**(10): p. 8488-98.
- 497 11. Yosinobu Onuma, P.W.S., *Bioresorbable Scaffold: The Advent of a New Era in* 498 *Percutaneous Coronary and Peripheral Revascularization?* Circulation, 2011. **123**: p. 499 779-797.
- 500 12. Roman Tsaryk, K.P., Susanne Barth, Ronald E. Unger, Dieter Scharnweber, C. James 501 Kirkpatrick, *The role of oxidative stress in pro-inflammatory activation of human* 502 *endothelial cells on Ti6Al4V alloy*. Biomaterials, 2013. **34**: p. 8075-8085.
- 503 13. D. Lison, P.C., L. Mollo, R. Lauwerys and B. Fubini, *Physicochemical mechanism of* 504 *the interaction between cobalt metal and carbide particles to generate toxic activated* 505 *oxygen species*. Chemical Research in Toxicology, 1995. **8**(4): p. 600-606.
- 506 14. Pierre-Alexis Mouthuy, S.J.B.S., Stephanie G. Dakin, Lidija Milkovi, Ana Cipak 507 Gasparovi, Andrew J. Carr, Neven Zarkovi, *Biocompatibility of implantable* 508 *materials: An oxidative stress viewpoint*. Biomaterials, 2016. **109**: p. 55-68.
- 509 15. Freyria, F.S., et al., *Hematite nanoparticles larger than 90 nm show no sign of toxicity* 510 *in terms of lactate dehydrogenase release, nitric oxide generation, apoptosis, and* 511 *comet assay in murine alveolar macrophages and human lung epithelial cells*. Chem 512 Res Toxicol, 2012. **25**(4): p. 850-61.
- 513 16. William T. Wallace, L.A.T., Yang Liu, Bonnie L. Cooper, David S. McKay, and 514 a.A.S.J. Bo Chen, *Lunar dust and lunar simulant activation and monitoring*. 515 Meteoritics & Planetary Science, 2009. **44**(7): p. 961–970.
- 516 17. Scott M. Wasserman, F.M., Laszlo G. Komuves, Ruey-Bing Yang, James E. 517 Tomlinson, Ying Zhang, Frank Spriggs, and James N. Topper, *Gene expression*

- 518 *profile of human endothelial cells exposed to sustained fluid shear stress*. *Physiol*
519 *Genomics*, 2002. **12**: p. 13-23.
- 520 18. Emily R. Shearier, P.K.B., Weilue He, Adam Drelich, Jaroslaw Drelich, Jeremy
521 Goldman, and Feng Zhao, *In Vitro Cytotoxicity, Adhesion, and Proliferation of*
522 *Human Vascular Cells Exposed to Zinc*. *ACS Biomater Sci Eng.*, 2016. **2**(4): p. 634–
523 642.
- 524 19. Francesco Turci, I.C., Gabriele Alberto, Gianmario Martra, Bice Fubini, *Free-radical*
525 *chemistry as a means to evaluate lunar dust health hazard in view of future missions*
526 *to the moon*. *Astrobiology*, 2015. **15**(5).
- 527 20. Bo Shen, R.C.J., and Hans Bohnert, *Mannitol Protects against Oxidation by Hydroxyl*
528 *Radicals*. *Plant Physiol.*, 1997.
- 529 21. Ranguelova, K. and R.P. Mason, *The fidelity of spin trapping with DMPO in*
530 *biological systems*. *Magn Reson Chem*, 2011. **49**(4): p. 152-8.
- 531 22. Ribes, S., et al., *Toll-like receptor stimulation enhances phagocytosis and*
532 *intracellular killing of nonencapsulated and encapsulated Streptococcus pneumoniae*
533 *by murine microglia*. *Infect Immun*, 2010. **78**(2): p. 865-71.
- 534 23. Capek, J., et al., *Microstructural, mechanical, corrosion and cytotoxicity*
535 *characterization of the hot forged FeMn30(wt.%) alloy*. *Mater Sci Eng C Mater Biol*
536 *Appl*, 2016. **58**: p. 900-8.
- 537 24. Cheng, J., et al., *Comparative in vitro Study on Pure Metals (Fe, Mn, Mg, Zn and W)*
538 *as Biodegradable Metals*. *Journal of Materials Science & Technology*, 2013. **29**(7): p.
539 619-627.
- 540 25. Xinhua Qu, L.J.K.a.E.T.B., *Hydroxyterephthalate as a Fluorescent Probe for*
541 *Hydroxyl Radicals: Application to Hair Melanin*. *Photochemistry and Photobiology*,
542 2000. **71**(3): p. 307-313.
- 543 26. V. Sansone, D.P., M. Melato, *The effects on bone cells of metal ions released from*
544 *orthopaedic implants. A review*. *Clinical Cases in Mineral and Bone Metabolism*,
545 2013. **10**(1): p. 34-40.
- 546 27. Roman Tsaryk, M.K., Ute Hempel, Dieter Scharnweber, Ronald E. Unger, Peter
547 Dieter, C.James Kirkpatrick, Kirsten Peters, *Response of human endothelial cells to*
548 *oxidative stress on Ti6Al4V alloy*. *Biomaterials*, 2007. **28**: p. 806-813.
- 549 28. F. Billi, P.C., *Nanotoxicology of metal wear particles in total joint arthroplasty: a*
550 *review of current concepts*. *Journal of Applied Biomaterials & Biomechanics*, 2010.
551 **8**(1): p. 1-6.
- 552 29. Ioannis Polyzois, D.N., Ioannis Michos, Efstratios Patsouris and Stamatis
553 Theocharis, *Local and systemic toxicity of nanoscale debris particles in total hip*
554 *arthroplasty*. *Journal of Applied Toxicology*, 2012. **32**: p. 255–269.
- 555 30. F L Nie, Y.F.Z., S C Wei, C Hu and G Yang, *In vitro corrosion, cytotoxicity and*
556 *hemocompatibility of bulk nanocrystalline pure iron*. *Biomedical Materials*, 2010. **5**.
- 557 31. Cheng, J., T. Huang, and Y.F. Zheng, *Microstructure, mechanical property,*
558 *biodegradation behavior, and biocompatibility of biodegradable Fe-Fe2O3*
559 *composites*. *J Biomed Mater Res A*, 2014. **102**(7): p. 2277-87.
- 560 32. Chen, K. and J.F. Keaney, Jr., *Evolving concepts of oxidative stress and reactive*
561 *oxygen species in cardiovascular disease*. *Curr Atheroscler Rep*, 2012. **14**(5): p. 476-
562 83.

563